

flexgrid2vec: Learning Efficient Visual Representations Vectors

Ali Hamdi, Flora Salim, and Du Yong Kim,

Abstract—We propose *flexgrid2vec*, a novel approach for image representation learning. Existing visual representation methods suffer from several issues, including the need for highly intensive computation, the risk of losing in-depth structural information and the specificity of the method to certain shapes or objects. *flexgrid2vec* converts an image to a low-dimensional feature vector. We represent each image with a graph of flexible, unique node locations and edge distances. *flexgrid2vec* is a multi-channel GCN that learns features of the most representative image patches. We have investigated both spectral and non-spectral implementations of the GCN node-embedding. Specifically, we have implemented *flexgrid2vec* based on different node-aggregation methods, such as vector summation, concatenation and normalisation with eigenvector centrality. We compare the performance of *flexgrid2vec* with a set of state-of-the-art visual representation learning models on binary and multi-class image classification tasks. Although we utilise imbalanced, low-size and low-resolution datasets, *flexgrid2vec* shows stable and outstanding results against well-known base classifiers. *flexgrid2vec* achieves 96.23% on CIFAR-10, 83.05% on CIFAR-100, 94.50% on STL-10, 98.8% on ASIRRA and 89.69% on the COCO dataset.

Index Terms—Visual Representation Learning, Graph Neural Networks.

I. INTRODUCTION

REPRESENTATION learning is a fundamental problem in computer vision. Convolutional Neural Networks (CNNs) have been used to learn image features in multiple visual applications. CNNs learn representative image convolutions through receptive fields to capture context information. However, CNNs are limited to local regions and affected by their isotropic mechanism [1]. These challenges make CNNs unable to cope directly with useful structural information of an image or to deal with diverse backgrounds and unrepresentative regions. Therefore, we describe the best solution to learn the convolutions only for the useful image segments (patches) while preserving the overall structural information. To this end, the image may be represented in a graph that has its nodes represent image patches or regions. However, CNNs cannot directly deal with such a graph of irregular structures.

Multiple techniques have tried to represent an image as a graph to harness the power of representation learning, such as part-based [2], region-based [3], pre-defined skeleton [4] and patch-based grid-graph [5]. Recently, Graph Convolutional Neural Networks (GCN) has been utilised to implement deep

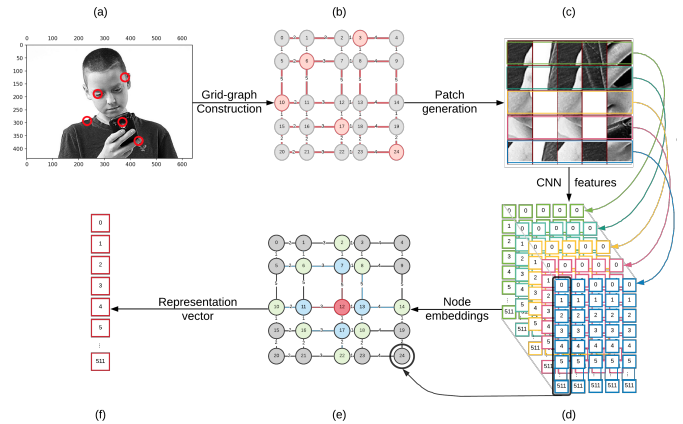


Fig. 1. *flexgrid2vec* consists of multiple components: (a) Extracts the image key-points. (b) Visualises the node projection and the constructed grid-graph. (c) Generates patches around node key-points. (d) Computes the convolution features. (e) Computes node embeddings learnt with neighbourhood features. (f) Produces the final features vector.

convolution networks over graphs. These approaches outperform CNN in encoding long relations between image regions [3]. However, these approaches suffer from several issues, such as losing significant local structures and the need for high computation resources. Graph models were developed for visual tasks with multiple objects in an image, such as object detection [6], tracking [2], action recognition [7], person search [8], face clustering [9], human pose estimation [10], multi-label image recognition [11] and segmentation [9]. Constructing a graph in these applications is simple as the semantic components are known in labelled images. However, there is difficulty in dealing with the whole image with no pre-defined semantic labels. The proposed *flexgrid2vec* solves this issue by handling the image as a grid-graph, combined with the power of GCN for visual image classification.

We propose *flexgrid2vec*, which constructs graph nodes only of informative image patches. We locate each graph node on a grid with original image coordinates. Our proposed design maintains the advantages of the global structure of the 2D grid, the local structure of the superpixels or region-based graphs and the flexible structure of the skeleton-based methods. Fig. 1 shows the main components of the proposed *flexgrid2vec*. It converts an image to a feature vector through a 2D grid-graph that aggregates the node embeddings using multiple CNNs. *flexgrid2vec* incorporates a set of novel contributions, as follows:

- A visual representation learning approach provides compact image representations considering significant image

Ali Hamdi and Flora Salim are with the School of Computing Technologies, RMIT University, Australia, ali.ali@rmit.edu.au, flora.salim@rmit.edu.au.

Du Yong Kim is with the School of Engineering, RMIT University, Australia, duyong.kim@rmit.edu.au.

Manuscript received September 27, 2021; revised 15 January 2022.

- patches and preserving their spatial relations on the grid.
- An effective method for learning node embeddings using GCN learnt with neighbourhood features.
- A comparative study on multiple image classification tasks with well-known baseline architectures and embedding methods on five benchmark datasets, namely CIFAR-10, CIFAR-100, STL-10, ASIRRA and COCO.

The rest of this paper is organised as follows. The related works are discussed in Section II. Section IV explains the components of the proposed *flexgrid2vec*. Sections VI and VII show the experiment results and work conclusions, respectively.

II. RELATED WORK

We discuss recent developments of CNN and GNN architectures for image representation. We then review related work in graph representation to highlight the significance of our proposed method in terms of flexibility and expressiveness.

A. Convolutional Neural Networks.

Recently, many CNN architectures have been widely used to learn image representations, such as VGG [12], ResNets [13], [14], [15], DenseNet [16], MobileNet [17], [18], and NASNet [19]. The performance of these models depends on the training data, network architecture, and loss function. These models are trained on large scale image datasets, e.g., ImageNet. CNNs employ different data augmentation techniques to achieve high accuracy and solve overfitting issues [20]. CNN models are being developed to have deeper structures to tackle the increasing size and complexity of training data. The CNN loss functions are being developed to compute effective gradients to learn the most discriminative convolution features. A large body of research in computer vision uses the CNNs, as mentioned earlier, as base models to achieve different visual representations [21], [22], [23] tasks. Recently, these CNNs have advanced image classification accuracy. For example, [13] achieved high accuracy in different image recognition tasks such as localisation and detection using ImageNet and COCO datasets. However, CNNs neglect useful structures due to the limitations of their receptive fields and isotropic mechanism [1].

B. Graph Neural Networks.

GCN aims to generalise the CNN to accommodate the non-euclidean graph data. GCN includes spectral and non-spectral representations. Spectral representations depend on graph polynomial, eigenvalues, and eigenvectors [24], [25]. This process requires extreme computations and results in structure-dependent representations [5]. Non-spectral GCN approaches operate directly on graph spatial neighbours. They adapt with vary-sized neighbourhoods to preserve the advantage of local invariance of the CNN [26]. GCN models have utilised in different computer vision tasks such as spatiotemporal graph for video analyses [27], [28], action recognition [4], [29], and person re-identification [30]. GCN is combined with Recurrent Neural Networks on cyclic variations of directed

graphs to model moving objects [31]. GCN has been combined with Haar transforms [32], [33], attention mechanism [34], Bayesian networks [35], adversarial auto-encoders [36]. GCN is also utilised with Siamese networks for object tracking [2], [37], [38]. However, to our knowledge, no GCN work considers the whole image representation. This paper proposes to encode the 2D image into a feature vector based on flexibly constructed grid-graphs.

C. Graph Representation Methods.

The main contribution of this paper is a new image representation learning method. This idea extends many previous graph construction techniques, such as part-based [2], region-based [3], pre-defined skeleton [4], and patch-based grid-graph [5]. Table II-C lists descriptions, applications, and limitations of these different graph designs. The part-based approach divides the image into a set of segments or patches [2]. These segments are used to construct graph nodes and edges. This approach depends on the spectral graph representation and node embedding to perform visual recognition. However, it loses significant local contextual structures. Region-based, not only with graphs, approaches use image regions for contextual reasoning and perception. They cluster similar image pixels into coherent regions. Graph structures are utilised to model various contexts for image recognition. Region-based approaches for graph representation outperform CNN in encoding long relations between image regions [3]. Pre-defined skeleton-based methods are limited to certain shapes such as the human body based on annotated joints or coordinates [4]. Another solution is to construct a grid-graph using non-overlapped patches [5]. The latter approach aims to reduce the number of graph nodes resulting in lower computation cost. However, this approach lacks a deep knowledge of the local structures. We propose *flexgrid2vec* that takes the advantages of the global structure of the 2D grid-graphs, local structure of the superpixels or region-based graphs, and flexible structure of the skeleton-based methods.

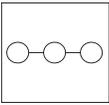
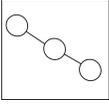
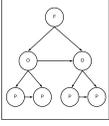
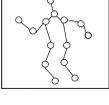
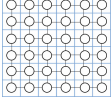
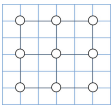
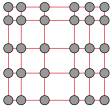
III. OVERVIEW

Visual recognition methods aim to learn discriminative image features that are useful in different downstream tasks, such as image classification. Existing methods, e.g. CNN-based, suffer from producing poor representation vectors due to challenges such as noise backgrounds and unrepresentative descriptors. For examples, Fig. 2 shows different images where the background covers large spans in (a and b) or shares colours with the foreground object in (c and d). Moreover, in Fig. 1 (a), the background has no useful information about the image. In this paper, we define the best visual representation method to learn only the important patches and their spatial relationships in an image. We propose *flexgrid2vec*, a novel GCN architecture to identify the important *local* patches and connect them through a graph to capture the *global* information.

IV. ARCHITECTURE: *flexgrid2vec*

We propose, *flexgrid2vec*, an algorithmic framework for visual representation learning. It aims to learn CNN features

TABLE I
A COMPARISON BETWEEN THE EXISTING GRAPH CONSTRUCTION METHODS.

Graph	Description	Applications	Limitations	Design
Part-based or Patch-based graph [2]	Segment the image into several parts or patches, each of which is represented by a node in the graph	Object tracking.	Loos informative local structures.	
Region-based or Superpixels graph [3], [39]	Group similar pixels into a set of groups (superpixels) and construct graph nodes for each group.	Object detection. Saliency detection. Segmentation. Semantic object parsing.	Loos informative local structures.	
Tree graph [40], [41]	An image is represented as a tree graph. A root node refers to the image. Child nodes represent the major components of the images. Leaf nodes are the image pixels.	Face recognition. Image segmentation.	Hard coded. High-cost computation.	
Skeleton [4]	Search for a skeleton point such as the human body.	Human body recognition.	Hard coded. Shape-dependent.	
Pixel-level grid-graph [42]	Construct a graph node for each pixel in the image.	Image classification.	High-cost computing.	
Patch grid-graph [5]	Construct a 2D grid-graph node for patches of non-overlapped pixels in the image.	Image classification. Person re-identification.	High-cost computing.	
flexgrid2vec (Ours)	Detect representative features, e.g., strong edges or key-points, and build the graph nodes using these points.	Image classification.	Dependent on the quality of key-point detectors.	

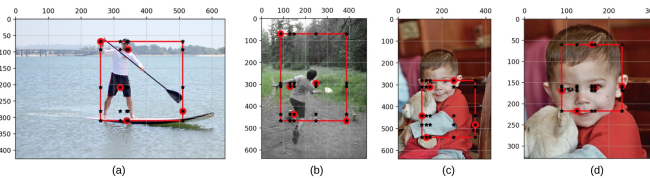


Fig. 2. *flexgrid2vec* generates Flexible Grid-Graphs for different image positions.

through a novel GCN architecture. We consider an image I as a grid-graph $G = (V, E)$ that consists of a set of nodes (image patches) and edges. The node coordinates and edges distances are flexible, i.e. dynamically changing from one image to another. *flexgrid2vec* converts this grid-graph into

a discriminative feature vector $f(I)$ as follows:

$$f(I) = \sum_{v \in V} \sum_{e \in E(v)} \varphi(v, e) \quad (1)$$

where $E(v)$ denotes the edges of the current node and $\varphi(v, e)$ is a GCN network that aggregates the CNN features from the neighbour nodes based on the grid connecting edges E . Table II lists the used notations. The $\varphi(v, e)$ is implemented to compute $H \in R^{n \times b}$, the node embeddings considering different edge attributes as in Eq. 5. *flexgrid2vec* includes three main steps:

- 1) Grid-graph construction.
- 2) Feature extraction through multiple CNNs.
- 3) Embeddings learning via GCN.

TABLE II
USED NOTATIONS.

Notation	Description	Notation	Description
G	Graph	V	The set of nodes.
v	A node $v \in V$.	E	The set of edges in a graph.
e_{ij}	An edge $e_{ij} \in E$.	$N(v)$	The neighbours of a node v .
$u \in N(v)$	A neighbour of v .	$z \in N(u)$	A 2-step neighbour of v , neighbour of neighbour.
n	The number of nodes, $n = V $.	m	The number of edges, $m = E $.
d	The dimension of a node feature vector.	$X \in R^{n \times d}$	The feature matrix of a graph.
$x_v \in R^d$	The feature vector of the node v .	b	The dimension of a hidden node feature vector.
$H \in R^{n \times b}$	The node hidden feature matrix.	$h_v \in R^b$	The hidden feature vector of node v .
c	The dimension of an edge feature vector.	$X^e \in R^{m \times c}$	The edge feature matrix of a graph.
y	The actual label.	\hat{y}	The predicted label.

A. Grid-graph Construction

flexgrid2vec represents an input image in the form of a flexible grid-graph. We select candidate key-points (pixels) that will be used to initialise the graph node coordinates. Fig. 1 (a and b) visualise the detected key-points using the Oriented FAST and Rotated BRIEF ORB algorithm [43]. ORB uses a patch intensity centroid to compute corner orientation, according to Eq. 2 and 3, where $I(x, y)$ is the image intensity at the coordinate (x, y) , p and q are the descriptive image moments and C is the centroid.

$$m_{pq} = \sum_{x,y} x^p y^q I(x, y) \quad (2)$$

$$C = \left(\frac{m_{10}}{m_{00}}, \frac{m_{01}}{m_{00}} \right) \quad (3)$$

where m_{00} denotes the area or volume of the image pixels, m_{10} is the sum over x and m_{01} refers to the sum over y . We use ORB to select a large set of pixels that covers the whole image. In some cases, ORB is not able to find enough key-points. Thus, a random set of pixels is used. Then, we utilise the K-means clustering approach to group this large set of pixels into a small set, as in Fig. 3. The selected pixels are used as the graph nodes. The coordinates of these nodes contribute to the graph *flexibility* in the same class through various images. For example, Fig. 2 (a, b, c and d) represent the graphs for different people while having unique spatial distributions of the nodes. They also contribute to the scene identities. For example, although human faces in Fig. 1 (a) and 2 (d) have quite different graph representations, they are still similar in comparison to the full-body graphs in Fig. 2 (a, b and c). In the next stage, we generate image patches for the graph nodes (selected pixels). Rublee et al. (ICCV 2011) report experiment results that support our selection, as follows:

- Detection time per frame (ms): ORB (15.3), SURF (217.3) and SIFT (5228.7).
- ORB had the best detection performance on synthetic data with more than 70% inliers, followed by SIFT, which dropped by 10%.
- On a real outdoor dataset: ORB (45.8%), SURF (28.6%) and SIFT (30.2%).

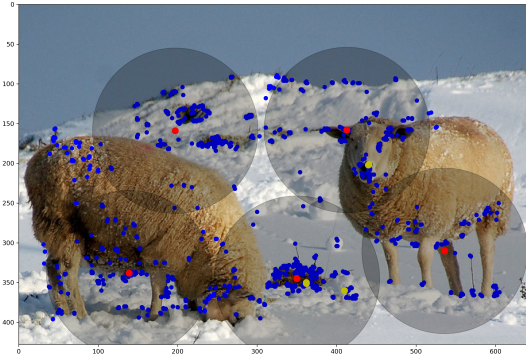


Fig. 3. The proposed key-point detection method has two phases, 1) ORB detects a large set of high-quality points (blue) and 2) K-means clusters them into a few clusters (red). These final points (red) are significantly representing the different image regions. This can be compared with the ORB outcome of few points (yellow).

B. Feature extraction through multiple CNNs

This work aims to reduce the learning of visual space to the most representative image patches. *flexgrid2vec* extracts the features for only a pre-defined small number of patches. These patches are centred around the above-mentioned key-point detection method (i.e. combining ORB and clustering). We slice a square patch of pixels around the centre of each node, as shown in Fig. 1 (f). This process tends to eliminate the insignificant or unrepresentative image parts, as can be seen in Fig. 1 (c). The generated patches represent all different essential regions in the original image in Fig. 1 (a). The overall size of the generated patches is tiny compared to the size of the original image.

flexgrid2vec then extracts convolution features for each patch. We utilise a CNN pre-trained on the ImageNet. This network can be replaced by any traditional image feature extraction method, such as histograms of gradients or colours. The extracted convolutional features are embedded in their node in a singularity model. These node features represent the graph nodes' attributes used to compute the node embedding H .

C. Embeddings Learning via GCN

This section explains the general GCN architecture used in the literature and the proposed *flexgrid2vec* GCN architecture.

1) *GCN*.: The learning process of GCN depends on two functions, including node embedding and output learning. GCN aims to learn the graph G embeddings as $H \in R^{n \times b}$, which comprises the neighbourhood information of the graph nodes V . The state $h_v \in R^b$ represents the node v embedding

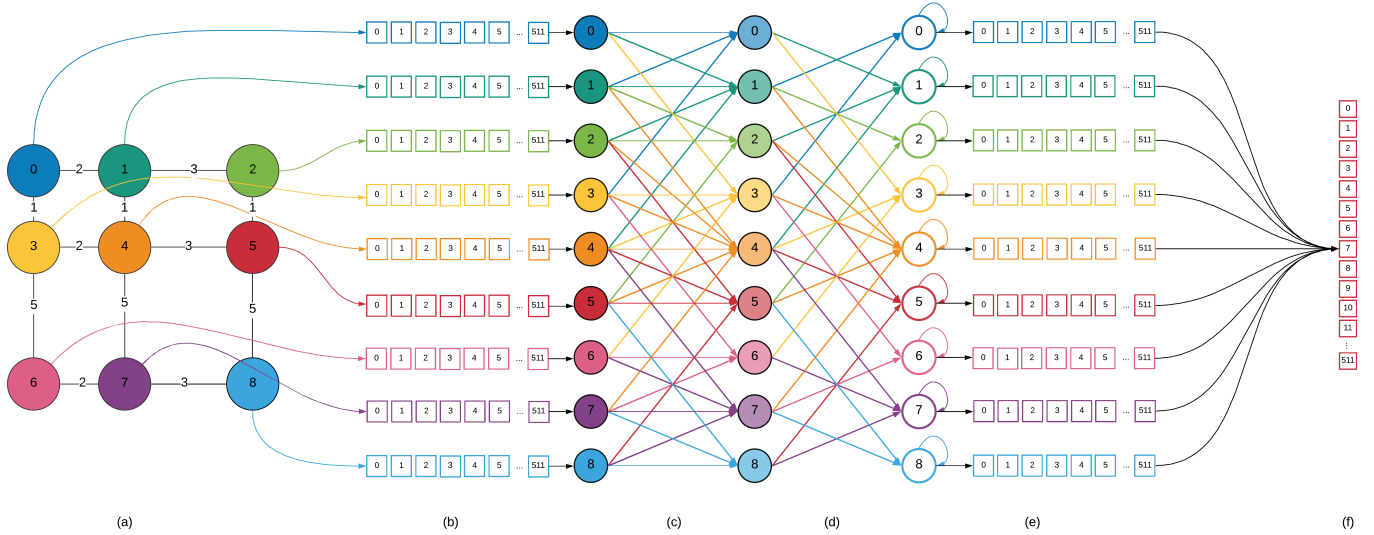


Fig. 4. *flexgrid2vec* node aggregation. (a) shows an example of a nine-node image. (b) CNN features as input to the embedding network. (c) aggregating the features of each node’s neighbours. (d and e) calculate the output vector of each node. (f) the sum of all graph vectors into the final representation vector.

in a b -dimension vector. This process can be defined as a parametric local transition function. This function is shared among all nodes and updates the node embeddings based on the input from the neighbourhood. Specifically, this function computes the node embedding using the node’s features, edges and neighbour information. The second main function is to learn the output label of each node. The embedding and output functions can be defined as follows:

$$h_v = \sum_{u \in N(v)} f(x_v, x_{(v,u)}^e, h_u, x_u) \quad (4)$$

where h_v is the embedding state of the node v , x_v are the node features, $x_{v,u}^e$ the feature vector of the edge between the node v and its neighbour u , and h_u and x_u are the embeddings and features of neighbourhood nodes. The aggregation of these embeddings can be computed as follows:

$$h_v = X_v \frac{\eta_n^T}{\varepsilon_v} + \sum_{u \in N(v)} X_u \frac{\eta_u^T}{\varepsilon_u} + \sum_{z \in N(v)} X_z \left(\frac{\eta_z^T}{\varepsilon_z} \right)^{\frac{1}{2}} \quad (5)$$

where X_n denotes the CNN features of the node patch, η_n^T is the transpose of the eigenvector of the node, X_u represents CNN-based features of the node neighbour $N(v)$, ε is the eigenvalue of the current node, $N(u)$ represents the neighbours of the current node’s neighbours and X_z is the features of the neighbour z . One possible solution to compute the eigenvectors is to use a Fourier basis. Fourier basis eigenvectors and their corresponding eigenvalues represent the direction and variance of the graph Laplacian. The decomposed eigenvectors are a matrix $U \in R^{n \times n}$ that contains η_n , where n dimension is the same as the node counts. These eigenvectors have a natural signal-frequency interpretation for the graph. The spectral Fourier basis decomposition produces the matrix U that diagonalises the Laplacian as follows:

$$L = \text{diag}(A + I)^{-1} = U \Lambda U^T \quad (6)$$

where Λ is a diagonal matrix of non-negative real eigenvalues. However, the calculation of the Fourier basis eigenvectors requires high-cost computations. Therefore, we propose to utilise the eigenvector centrality scores.

Then, the output function is computed as follows:

$$o_v = g(h_v, x_v) \quad (7)$$

where g is a local function that describes the node output label. By stacking the versions of f and g for all nodes, we get F and G , which are the global transition and output functions. GCN uses a gradient-descent algorithm for the learning process with $loss = \sum_{i \in n} (y_i - \hat{y}_i)$, where n is the number of labelled nodes and y and \hat{y} represent the target and output labels, respectively. Finally, the learnt node embeddings are concatenated in one vector to represent the given image. However, this generic GCN architecture is not applicable in our use-case. To represent an image as a vector, we do not have different node labels. Therefore, we model the GCN on our proposed *flexgrid2vec*, as explained below.

2) *The proposed GCN.*: *flexgrid2vec* defines the grid-graph as $G = (V, E)$ of nodes V and edges E . The goal of the proposed GCN is to learn the embedding state $h_v \in R^b$. *flexgrid2vec* uses the node attributes, i.e. the CNN-based extracted features, to learn the node embeddings $H \in R^{n \times b}$. *flexgrid2vec* constructs the grid-graph as a flexible skeleton where the graph edges are attributed by the distance between the nodes as $E_{v,u} = \text{distance}(v, u)$. Therefore, the edges mostly have different lengths.

To this end, we have defined the grid-graphs, its nodes and node features, and its edges and edge attributes. Next, we define each node’s neighbourhood and compute the node embeddings $H \in R^{n \times b}$. *flexgrid2vec* computes the node embedding based on the node CNN features, as follows:

$$h_v = X_v + \sum_{u \in N(v)} X_u \frac{\gamma}{\theta} + \sum_{z \in N(u)} X_z \frac{\gamma}{\theta} \quad (8)$$

where X_v and X_u denote the CNN features of the current node patch and the node neighbours $N(v)$, $N(u)$ represents the neighbours of neighbours, X_z are the features of the neighbour and $\frac{\gamma}{\theta}$ is a normalisation factor. This normalisation process aims to scale the embedding features into a specific range. The γ and θ variables can be pre-defined or computed based on the spectral graph theory.

We investigate the impact of using the spectral graph components on the embedding vectors. The embedding computing methods in Eq. 8 will be updated as follows:

$$h_v = X_v c_v + \sum_{u \in N(v)} \frac{X_u c_u}{\theta} + \sum_{z \in N(u)} \frac{X_z c_z}{\theta} \quad (9)$$

where c_v and c_u are the eigenvector centrality scores of the node and its neighbours. Eigenvector centrality calculates the centrality score C for each node based on its neighbours. Eigenvector centrality is an extension of the simple degree centrality. Degree centrality is an awarding mechanism giving one centrality point for every neighbour in the graph. Eigenvector centrality considers the importance level of each neighbour. The node importance increases or decreases based on the importance of its neighbours. Eigenvector centrality assigns each node a score proportional to the sum of its neighbours' scores as follows:

$$c_v = \varepsilon_l^{-1} \sum A_{v,u} c_u \quad (10)$$

where c_v represents the centrality of the node v , ε_l is the largest eigenvalue, $A_{v,u}$ is an element in the adjacency matrix and c_u is the neighbour node. In this scenario, for graph convolution, Eq. 8 concatenates + the aggregated sum of the node neighbours and their neighbours. This operation limits the convolution as a two-step aggregation process. In this paper, we will test different versions of Eq. 8 and 9.

To this end, we introduced the main components of *flexgrid2vec*, including the construction of the Flexible Grid-Graphs and learning the node embeddings. In the following sections, we discuss the experiment results for each component.

V. EXPERIMENT SETTINGS

A. Implementation Details

We used multiple Python packages to implement the different components of *flexgrid2vec*, including, 1) Grid-graph construction, 2) Feature extraction through multiple CNNs and 3) Embeddings learning via GCN. We conducted all experiments in a HPE NVIDIA Tesla V100 GPU server with 512GB memory.

The following are the model parameter settings:

- **Key-point detection.** The key-point detection method is parameterised by two variables, including the ORB key-point numbers and the output clusters (key-pixels). We specified the feature number to be 250, as shown in blue in Fig. 3. Then, we used K-means clustering to select the most representative 5 clusters, i.e. points, as visualised in red in Fig. 1 (c).
- **Grid-graph construction.** We constructed a grid-graph based on the coordinates of the detected key-pixels.

- **Patch Generation.** We generated 5×5 patches of size 32×32 centred around the detected key-pixels. The generated patches were a total of 25 patches (25,600 pixels) instead of the original image-size of 438×640 (280,320 pixels). The pixel rate was reduced by around 91% of the original image.
- **CNN Feature Extraction.** We employed the TensorFlow pre-trained VGG model to extract the X_v convolutional features for each v node.
- **GCN embedding setting.** The most optimal setting for the GCN embedding is aggregating the node CNN features on a one-step neighbourhood, denoted as *flexgrid2vec-Agg1R*. We have investigated multiple node-embedding methods as explained below.

B. Different Embedding Configurations

We implemented *flexgrid2vec* using various embedding aggregation methods. These methods are as follows:

- 1) *flexgrid2vec-Agg1R* computes the node feature embeddings by aggregating the direct connected neighbours. It then takes the sum of the 25 node vectors to represent the image in a 1×512 feature vector. The node embedding method in Eq. 8 will be defined as follows: $h_v = X_v + \sum_{u \in N(v)} \frac{X_u}{\theta}$.
- 2) *flexgrid2vec-Agg1* computes the node feature embeddings by aggregating the direct connected neighbours. The aggregated vectors are concatenated as one vector. For example, a 5×5 grid-graph that has 25 nodes will have 25×512 features concatenated in the output vector. The node embedding method in Eq. 8 will be defined as follows: $h_v = X_v \curvearrowright \frac{X_u}{\theta} \forall u \in N(v)$.
- 3) *flexgrid2vec-Agg2R* computes the sum of the vectors of the current node's neighbours and their neighbours. It follows the same node embedding method in Eq. 8.
- 4) *flexgrid2vec-Agg2* works like *flexgrid2vec-Agg2R* but with concatenation instead of summation. The node embedding method in Eq. 8 will be defined as follows: $h_v = X_v \curvearrowright \frac{X_u}{\theta} \forall u \in N(v) \curvearrowright \sum_{z \in N(u)} \frac{X_z}{\theta}$.
- 5) *flexgrid2vec-EVC1R* normalises the output of *flexgrid2vec-Agg1R* with the eigenvector centrality score. The node embedding method in Eq. 9 will be defined as follows: $h_v = X_v c_v + \sum_{u \in N(v)} \frac{X_u c_u}{\theta}$.
- 6) *flexgrid2vec-EVC1* normalises the output of *flexgrid2vec-Agg1* with the eigenvector centrality of the Flexible Grid-Graphs. The node embedding method in Eq. 9 will be defined as follows: $h_v = X_v c_v \curvearrowright \frac{X_u c_u}{\theta} \forall u \in N(v)$.
- 7) *flexgrid2vec-EVC2R* considers the two-step neighbour aggregation, normalisation with eigenvector centrality and vector size reduction via summation. It follows the same node embedding method as Eq. 9.
- 8) *flexgrid2vec-EVC2* extends the method of *flexgrid2vec-EVC1* to the neighbours of neighbours at only two steps. The node embedding method in Eq. 9 will be defined as follows: $h_v = X_v c_v \curvearrowright \frac{X_u c_u}{\theta} \forall u \in N(v) \curvearrowright \sum_{z \in N(u)} \frac{X_z c_z}{\theta}$.

Fig. 4 shows the main steps of the node aggregation process.

C. Datasets

Two datasets are considered to conduct experiments with *flexgrid2vec* on both visual representation learning and image classification tasks. Specifically, we used:

- 1) CIFAR-10 [44] consists of 60,000 images. The images are 32×32 in size and divided into 50,000 for training and 10,000 for testing. CIFAR-10 has 10 categories, such as aeroplane, automobile, bird, cat, deer, dog and frog. The categories are mutually exclusive with no overlapping.
- 2) CIFAR-100 [44] is similar to the CIFAR-10 but has 100 classes containing 600 images each.
- 3) STL-10 [45] was prepared for image recognition model evaluation. STL-10 has fewer labelled training examples and has 5,000 images for training and 8,000 for testing, over 10 classes, as well as 100,000 unlabelled images for unsupervised learning. However, in this paper, we did not use any of these unlabelled images. The STL-10 5,000 and 8,000 images are 96×96 and are acquired from the ImageNet.
- 4) ASIRRA (Animal Species Image Recognition for Restricting Access), published by Microsoft for binary classification, is a balanced dataset having, for each class, 12,500 and 1,000 images for training and testing, respectively.
- 5) COCO (Microsoft Common Objects in Context) dataset [46] for multi-class image classification has 123,287 images annotated for 80 object categories and 12 super categories. One image may be annotated to one or more object classes. We filter the dataset to images that are only annotated to one class. Therefore, the final utilised dataset is around 29,000 images for multi-class classification on 12 super categories. This utilised sub-set produces challenging issues of imbalanced and heterogeneous images. This heterogeneity stemmed from the utilisation of the super high-level categories: vehicles, indoor and accessories. The heterogeneity issue can be seen in multiple ways: different backgrounds as in the vehicle category, e.g. sea and grass; miscellaneous items as in the indoor class, e.g. vase and teeth brush; and various types as in accessories, e.g. bag and umbrella.

D. Baseline and State-of-the-art Methods

We compare the image classification results of *flexgrid2vec* with state-of-the-art CNN-based methods that are pre-trained on ImageNet, such as VGG [12], ResNets [13], [14], [15], DenseNet [16], MobileNet [17], [18], NASNet [19], Xception [47] and InceptionV3 [48]. We also compare the embedding method of the proposed *flexgrid2vec* with the existing embedding models: node2vec [49] and GCN-based aggregated nodes [50]. In addition, we compare *flexgrid2vec*'s accuracy with recent algorithms, such as MixMatch [51] (NIPS 2019), DIANet [52] (AAAI2020), reSGHMC [53] (ICML 2020), Prodpoly [54] (TPAMI 2021), ACNet [55] (CVPR 2019), Quadratic-Embedding [56] (ICLR 2020) and CLS-GAN [57], (IJCV 2020).

TABLE III
CLASSIFICATION ACCURACY (TOP 1) RESULTS ON CIFAR-10.

Model	Test Accuracy	Venue (Year)
DeepInfoMax (G) [58]	52.84%	ICLR 2019
Adversarial AutoEncoder [59]	57.19%	ICLR 2016
Variational AutoEncoder (VAE) [60]	60.54%	
ANODE [61]	60.6%	NeurIPS 2019
BiGAN [59], [62]	62.74%	
DeepInfoMax (infoNCE) [58]	75.57%	ICLR 2019
DenseNet [16]	77.79%	CVPR 2017
DenseNet (Spinal FC)	81.13%	
DCGAN [63]	82.8%	
Roto-Scat + SVM [64]	82.30%	
ExemplarCNN [65]	84.3%	
Baikal [66]	84.53%	CEC 2020
CapsNet [67]	89.4%	NeurIPS 2017
MP [68]	89.07%	
MIM [69]	91.5%	WACV 2016
CLS-GAN [57]	91.7%	IJCV'2020
DSN [70]	91.8%	PMLR'15
BinaryConnect [71]	91.7%	NeurIPS 2015
Mish [72]	92.20%	BMVC 2020
SA quadratic embedding [56]	93.8%	ICLR 2020
Standard ACNet [55]	94%	CVPR 2019
Deep Complex [73]	94.4%	ICLR 2018
Prodpoly [54]	94.9%	TPAMI 2021
MixMatch [51]	95.05%	NEURIPS 2019
SRM-ResNet-56 [74]	95.05%	ICCV 2019
Evolution ensemble [75]	95.6%	ICML 2017
PreActResNet18+AMP [76]	96.03%	CVPR 2021
Wide Residual Networks [77]	96.11%	
ResNet20 with reSGHMC [53]	94.62%	ICML 2020
ResNet56 with reSGHMC [53]	96.12%	ICML 2020
flexgrid2vec	96.23%	

VI. EVALUATION

For evaluation purposes, we utilised *flexgrid2vec* to extract the feature vectors of two image datasets. Then, we developed a simple fully connected neural network to classify the images. In the following sub-sections, we discuss the performance of *flexgrid2vec* to show its efficiency and accuracy. We test *flexgrid2vec* as a visual representation algorithm. We visualise the produced vectors to highlight the learnt feature space. We also tested *flexgrid2vec* on binary and multi-class image classification tasks. Finally, we evaluate *flexgrid2vec* under different configurations and with multiple node-embedding methods. The architecture with the *AGGIR* embedding method showed the best results. Therefore, we refer to that version by *flexgrid2vec* in the rest of this paper.

A. Benchmarking Results

We compare the benchmarking results of *flexgrid2vec* with the state-of-the-art methods. Although *flexgrid2vec* produces

significantly reduced feature vectors, it has high classification accuracy. Tables III, IV, V, VI and VII list the learning test accuracy.

flexgrid2vec achieves 96.23%, outperforming baseline and state-of-the-art image classification methods, as listed in Table III. As *flexgrid2vec* is a batch-based visual representation, it is directly compared to DeepInfoMax [58]. DeepInfoMax has been implemented based on different configurations and loss functions. It has 52.84%, 70.60%, 73.62% and 75.57% accuracy. Also, *flexgrid2vec* outperforms recent advances in the state-of-the-art AutoEncoder (AE), such as Adversarial AE, Variational AE and β -VAE, which have achieved 57.19%, 57.89% and 60.54%, respectively. Table IV shows the experiment results on the CIFAR-100 dataset. *flexgrid2vec* achieves 81.47%, outperforming recent methods, such as ResNet-1001 [15], MixMatch [51], Mish [72] and DIANet [52]. On the other hand, the benchmark results on the STL-10 dataset show that the proposed *flexgrid2vec* outperforms different methodologies, such as GAN [59], Autoencoders [59], [60], [78], [79], [62] and patch-based DeepInfoMax [58].

In binary classification on the ASIRRA dataset, *flexgrid2vec* achieves 98.8%, outperforming all the state-of-the-art methods. In multi-class, on the COCO dataset, *flexgrid2vec* achieves 89.69%, having the first rank with the VGG19. The results of both binary and multi-class image classifications show the consistency of *flexgrid2vec*'s learning behaviour. *grdi2vec* learns smoothly in both tasks. Although some state-of-the-art algorithms achieve high accuracy, they show overfitting and fluctuation between the train and test results. For example, NASNetMobile has 98% in training and only 47% in testing. It appears they suffer from the challenging issues of the utilised dataset as discussed in the datasets section. This result confirms the superiority of *flexgrid2vec* as an efficient visual representation learning approach.

TABLE IV
CLASSIFICATION ACCURACY (TOP 1) RESULTS ON CIFAR-100.

Model	Test Accuracy	Venue (year)
DSN [70]	65.4%	PMLR 2015
Unsharp Masking [80]	60.36%	ICANN 2019
ResNet-50 [15]	67.06%	PMLR 2015
GFE [81]	67.7%	IJCNN 2015
MIM [69]	70.8%	WACV 2016
MixMatch [51]	74.10%	NIPS 2019
Mish [72]	74.41%	BMVC 2020
Stochastic Depth [14]	75.42%	ECCV 2016
Exponential Linear Units [82]	75.7%	
DIANet [52]	76.98%	AAAI2020
Evolution [75]	77%	ICLR 2017
ResNet-1001 [15]	77.3%	ECCV 2016
flexgrid2vec	83.05%	

The proposed *flexgrid2vec* distinguishes the most important patches to learn accurate representations that are effective with a small fraction of the image patches. In order to validate the proposed methodology, we utilise two high-resolution image sets, namely ASIRRA and COCO, achieving 98.8% and 82.38%, respectively. In order to compare *flexgrid2vec*

TABLE V
CLASSIFICATION ACCURACY (TOP 1) RESULTS ON STL-10.

Model	Test Acc.	Venue (Year)
Variational AutoEncoder (VAE) [60]	56.72%	ICLR 2014
AE	55.57	
β -VAE [78]	55.14%	ICLR 2017
Adversarial Autoencoders (AAE) [59]	54.47%	ICLR 2016
Noise As Target (NAT) [83]	61.43%	
DeepInfoMax (DV) [58]	63.81%	ICLR 2019
Accuracy Monitoring [84]	63.43%	IJCAI-PRICAI 2020
Hierarchical Matching Pursuit (HMP)[85]	64.5%	ICCV 2017
BiGAN [62]	67.18%	
DFF Committees [86]	68%	Pattern Recognition 2014
C-SVDDNet [87]	68.20%	Pattern Recognition 2016
DeepInfoMax (JSD) [58]	70.85%	ICLR 2018
ResNet18 [88]	72.66%	
Second-order Hyperbolic CNN [89]	74.3%	JMIV 2019
Exemplar CNN [85]	75.7%	ICCV 2017
Parabolic [89]	77%	JMIV 2019
PSLR-Linear [90]	78.8%	CVPR 2020
Greedy InfoMax [91]	81.9%	NeurIPS 2019
ResNet baseline [92]	82%	ECCV 2018
PSLR-knn [93]	83.2%	CVPR 2020
HybridNet [92]	84.10%	ECCV 2018
MidPoint [94]	84.6%	AAAI 2018
IIC [95]	88.8%	ICCV 2019
SESN [96]	91.49%	ICLR 2020
NSGANetV2 [97]	92.0%	ECCV 2020
FixMatch [98]	92.34%	NEURIPS 2020
AMDIM [99]	93.80%	ICML 2020
ReMixMatch [51]	93.82%	ICLR 2019
AMDIM-L [99]	94.2%	ICML 2020
MixMatch [51]	95.05%	NEURIPS 2019
flexgrid2vec (Ours)	94.50	

TABLE VI
BINARY CLASSIFICATION BENCHMARKING RESULTS ON ASIRRA DATASET.

Model	Test Accuracy	Test Loss
VGG16 [12]	82.2%	0.274
VGG19 [12]	88.2%	0.137
ResNet50 [13]	50%	0.502
InceptionV3 [48]	97.2%	0.032
DenseNet121 [16]	94.3%	0.073
MobileNet [18]	98.4%	0.023
NASNetMobile [19]	97.9%	0.022
flexgrid2vec (ours)	98.8%	0.049

with state-of-the-art algorithms on low-resolution datasets, such as CIFAR-10, CIFAR-100 and STL-10, we combined the feature vectors of *flexgrid2vec* with other baseline models, as shown in Table VIII. The table lists the results of using *flexgrid2vec* within different ablations on the five utilised datasets. Using *ResNet-50* in combination with *flexgrid2vec* achieves 94.50% and 82.38 to 89.74% accuracy using the STL-10 and COCO datasets, respectively. Table VIII also shows the impact of changing the image size. *flexgrid2vec*

TABLE VII
MULTI-CLASS CLASSIFICATION BENCHMARKING RESULTS ON COCO DATASET.

Model	Test Accuracy	Test Loss
VGG16 [12]	79.0%	0.738
VGG19 [12]	82.9%	0.620
ResNet50 [13]	61.26%	0.240
InceptionV3 [48]	60.5%	1.923
DenseNet121 [16]	75.05%	0.597
MobileNet [18]	70.7%	1.196
NASNetMobile (depth multiplier=1.0) [19]	59.28%	0.674
NASNetMobile (depth multiplier=0.5) [19]	62.60%	0.574
flexgrid2vec (ours)	89.69%	0.11

achieves better results on the STL-10 dataset when scaling the images up from 96 to 224. Increasing the patch size in the case of CIFAR-10 also improves the accuracy from 95.73% to 96.23%. Moreover, increasing both the image and patch sizes increases the accuracy of *flexgrid2vec* by around 2%. This trend can also be seen in COCO accuracy, which is increased by around 7%. However, implementing *flexgrid2vec* on the binary classification data achieves high accuracy without the need to be combined with other deep models.

Fig. 5 and 6 show the testing accuracy of *flexgrid2vec* on the CIFAR-10 and STL-10 datasets. We experimented with CIFAR-10 using the proposed *flexgrid2vec* in combination with ResNet-50 and EfficientNet with the same patch size of 32 pixels. The combination with ResNet-50 outperformed the one with EfficientNet by 2.25%. We also reduced the patch size from 32 to 20 using the ResNet-50. The latter experiment shows that the 32 setup has better accuracy, with 96.23% in comparison to 95.73% using the 20 pixel patch setup. Fig. 6 shows the impact of different image sizes using *flexgrid2vec* and ResNet-50. Using the image size of 224 pixels has the highest accuracy, though it fluctuates due to the large scaling from the original size of 32 pixels. On the other hand, using an image size of 96 pixels has less accuracy of 92.95% but a steady learning curve.

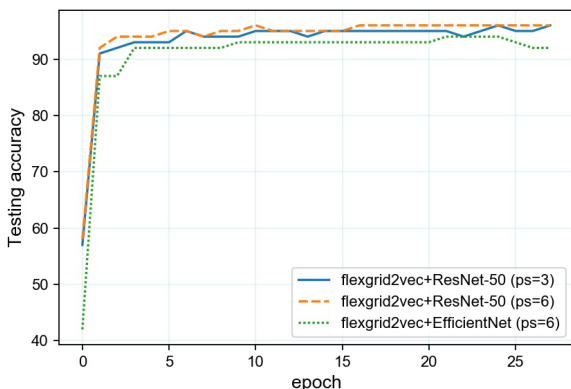


Fig. 5. Testing accuracy of *flexgrid2vec* on the CIFAR-10 dataset.

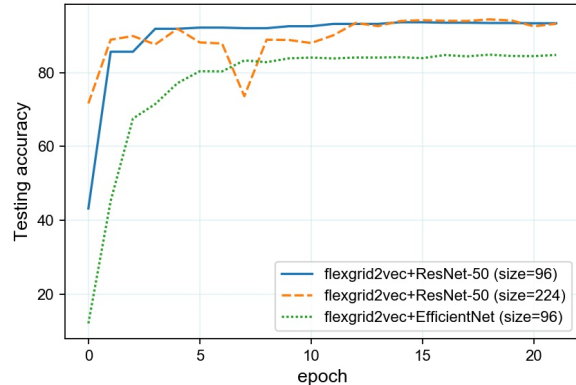


Fig. 6. Testing accuracy of *flexgrid2vec* on the STL-10 dataset.

B. Embedding Configuration

1) *flexgrid2vec* Embedding Configuration Testing: We conducted a large set of experiments to evaluate the performance of *flexgrid2vec*. Table IX lists sample results of model training using different embedding methods. The embedding calculation methods have different learning behaviours. Specifically, the methods that concatenate the output vectors as one large vector tend to have inferior test accuracy, showing around 9% less than the training accuracy. However, reduced vector-based methods show better learning behaviour for both training and testing. This significant performance of the reduced *flexgrid2vec* is caused by using the most discriminative 512 features instead of using a large vector of 12,800 features. The *flexgrid2vec-Agg1R* that applies simple node aggregation and summation outperforms all other versions including the method with eigenvector centrality normalisation. This observation proves that the *flexgrid2vec* requires lower computation to produce the best representation vector. The average speed highlights how fast *flexgrid2vec* is. The results show that *flexgrid2vec* processes around 20 images per second.

We evaluated the parameters of *flexgrid2vec*, such as the patch size and node count. Table X shows the performance results of building *flexgrid2vec* grid-graphs on 7 key-points (7×7 nodes). These results decreased by a range of 6 to 15 percent when using *flexgrid2vec* on five key-points (5×5 nodes), see Table IX. Table XI shows the training results of the *flexgrid2vec* reduced methods. These experiments were designed to utilise 64×64 patch sizes to calculate the convolutional feature of each node. The accuracy degraded significantly in all the methods. For example, the test accuracy of *flexgrid2vec-Agg1R* decreased from 98.8% to 90.1%. This result supports the strength of the *flexgrid2vec* proposed architecture that uses 32×32 patch sizes, see results in Table IX.

2) *Comparison with other embedding methods*: For benchmarking the embedding component of *flexgrid2vec*, we utilised the state-of-the-art node2vec [49] algorithm to compute the node embeddings. node2vec is useful to produce flexible node neighbourhoods. The neighbourhood design is biased to random walks. This process enables the algorithm to learn a

TABLE VIII
CLASSIFICATION ACCURACY (TOP 1) RESULTS ON DIFFERENT PARAMETER SETTINGS.

Dataset	Image Size	Base Model	Dimension	Patch Size	Test Acc.
<i>STL</i> – 10	96	ResNet50	4096	20	92.95%
	96	EfficientNet	18448	20	88.15%
	224	ResNet50	4096	8	94.50%
<i>CIFAR</i> – 10	32	ResNet50	1016	32	87.90%
	96	ResNet50	2048	32	96.23%
	96	EfficientNet	18448	32	93.98%
	96	ResNet50	2048	20	95.73%
<i>CIFAR</i> – 100	32	ResNet50	1016	32	63.88%
	96	ResNet50	2048	32	81.38%
	224	ResNet50	2048	32	83.05%
<i>ASIRRA</i>	224	None	None	32	98.8%
<i>COCO</i>	400	None	Noe	32	82.38%
	400	ResNet50	2048	32	89.74%

TABLE IX
EXPERIMENT RESULTS OF USING *flexgrid2vec* EMBEDDING METHODS WITH PATCH SIZE OF 32×32 .

Embedding Method	Test Acc.	Test loss	Time (s)
<i>Agg1R</i>	98.8%	0.049	0.051
<i>Agg1</i>	88.7%	0.115	0.053
<i>Agg2</i>	90.8%	0.093	0.074
<i>Agg2R</i>	96.8%	0.102	0.070
<i>EVC1</i>	88.8%	0.303	0.053
<i>EVC1R</i>	97.9%	0.069	0.050
<i>EVC2</i>	90.2%	0.1	0.076
<i>EVC2R</i>	96.1%	0.122	0.076

TABLE X
PERFORMANCE RESULTS OF *flexgrid2vec* WITH GRID-GRAPHS OF 7×7 (49) NODES.

Embedding Method	Test Acc.	Test loss	Time (s)
<i>Agg1R</i>	81.2%	0.398	0.402
<i>Agg1</i>	81.5%	0.135	0.412
<i>Agg2</i>	82.3%	0.144	0.401
<i>Agg2R</i>	79.7%	0.41	0.426
<i>EVC1</i>	80.3%	0.156	0.431
<i>EVC2</i>	80.4%	0.187	0.43
<i>EVC2R</i>	78.8%	0.409	0.455
<i>EVC1R</i>	79.5%	0.394	0.433

TABLE XI
PERFORMANCE RESULTS OF *flexgrid2vec* WITH PATCH SIZE OF 64×64 .

Embedding Method	Test Acc.	Test loss	Time (s)
<i>Agg1R</i>	90.1%	0.105	0.039
<i>Agg2R</i>	90%	0.227	0.053
<i>EVC1R</i>	90.9%	0.229	0.041
<i>EVC2R</i>	89.4%	0.263	0.057

low-dimensional feature space based on the skip-gram that is utilised in the deep-walk methodology [100]. The aim now is to maximise node neighbourhood log-probability, as in the following objective function:

$$\max_f \sum_{v \in V} \log \Pr(N(v)|f(v)) \quad (11)$$

The edge weights are used to bias the random walks to control the next node that will be considered in the neighbourhood. In addition, we also implemented a layer message aggregation network based on GCN [50]. The feature vector is computed based on the grid-graph representations.

Tables XII and XIII show that *flexgrid2vec* outperforms both models with high accuracy margins in both binary and multi-class image classification. *flexgrid2vec* has 25 and 10 percent more test accuracy in comparison to using GCN and node2vec.

TABLE XII
BENCHMARKING THE NODE EMBEDDING MODELS FOR BINARY CLASSIFICATION

Model	Test Accuracy	Test Loss
<i>flexgrid2vec</i> (node2vec)	73.0%	0.122
<i>flexgrid2vec</i> (GCN)	89.2%	0.271
<i>flexgrid2vec</i>	98.8%	0.049

TABLE XIII
BENCHMARKING WITH THE NODE EMBEDDING MODELS FOR MULTI-CLASS CLASSIFICATION

Model	Test Accuracy	Test Loss
<i>flexgrid2vec</i> (node2vec) [49]	36.4%	2.043
<i>flexgrid2vec</i> (GCN) [50]	70.3%	1.020
<i>flexgrid2vec</i>	89.74%	0.11

C. Visual Feature Representation

flexgrid2vec is a visual representation algorithm that represents an image as a feature vector. Fig. 7 and Fig. 8 show 2D visualisations of *flexgrid2vec* representations of two-class (*ASIRRA*) and 12-class (*COCO*) datasets. *flexgrid2vec* produces a 1×512 feature vector. We utilised principal component analysis (PCA) to reduce the dimensions for visualisation purposes. Fig. 7 highlights the superiority of *flexgrid2vec*'s performance. The given *ASIRRA* image dataset is successfully represented in a significant way. This high performance is supported by the classification accuracy. Fig. 8 shows the *flexgrid2vec* performance on the *COCO* image dataset. The given dataset is highly imbalanced, yet *flexgrid2vec* still produces discriminative features, as illustrated in Fig. 8.

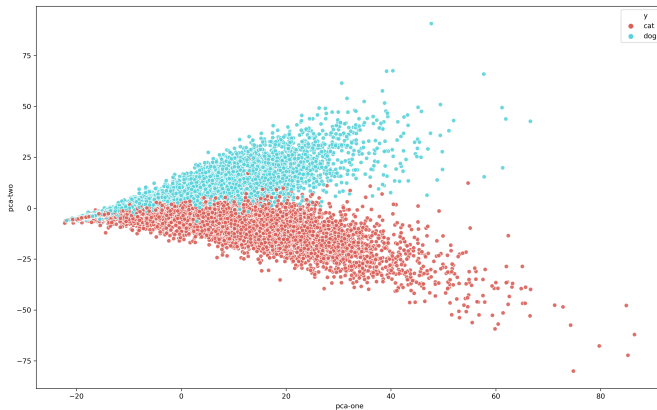


Fig. 7. PCA two-component visualisation of ASIRRA dataset *flexgrid2vec* vectors.

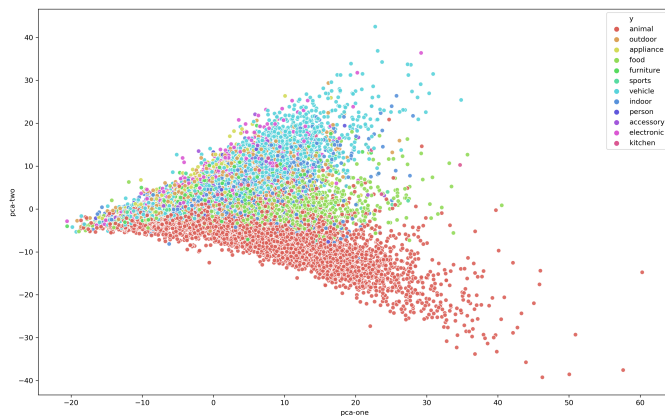


Fig. 8. PCA two-component visualisation of COCO dataset *flexgrid2vec* vectors.

VII. CONCLUSION

We propose a novel GNN-based approach to learn visual features, called *flexgrid2vec*. It learns feature representation through constructing grid-graphs that are flexible to the input image. The experiment results show the superiority of the proposed *flexgrid2vec* in both binary and multi-class image classification using reduced feature vectors. *flexgrid2vec* learns image features of only the most important patches. In the future, we will investigate the usage of *flexgrid2vec* for few-shot learning, visual segmentation and object detection. We will also research the utilisation of other loss functions, such as contrastive loss and data augmentation techniques.

ACKNOWLEDGMENTS

Ali Hamdi is supported by RMIT Research Stipend Scholarship. This research is partially supported by Australian Research Council (ARC) Discovery Project *DP190101485*.

REFERENCES

[1] W. Luo, Y. Li, R. Urtasun, R. Zemel, Understanding the effective receptive field in deep convolutional neural networks, in: *Advances in neural information processing systems*, 2016, pp. 4898–4906.

[2] J. Gao, T. Zhang, C. Xu, Graph convolutional tracking, in: *Proceedings of the IEEE Conference on Computer Vision and Pattern Recognition*, 2019, pp. 4649–4659.

[3] Y. Li, A. Gupta, Beyond grids: Learning graph representations for visual recognition, in: *Advances in Neural Information Processing Systems*, 2018, pp. 9225–9235.

[4] S. Yan, Y. Xiong, D. Lin, Spatial temporal graph convolutional networks for skeleton-based action recognition, in: *Thirty-Second AAAI Conference on Artificial Intelligence*, 2018.

[5] J. Zhou, G. Cui, Z. Zhang, C. Yang, Z. Liu, M. Sun, Graph neural networks: A review of methods and applications, *arXiv preprint arXiv:1812.08434* (2018).

[6] H. Xu, C. Jiang, X. Liang, Z. Li, Spatial-aware graph relation network for large-scale object detection, in: *The IEEE Conference on Computer Vision and Pattern Recognition (CVPR)*, 2019.

[7] C. Si, W. Chen, W. Wang, L. Wang, T. Tan, An attention enhanced graph convolutional lstm network for skeleton-based action recognition, in: *The IEEE Conference on Computer Vision and Pattern Recognition (CVPR)*, 2019.

[8] Y. Yan, Q. Zhang, B. Ni, W. Zhang, M. Xu, X. Yang, Learning context graph for person search, in: *The IEEE Conference on Computer Vision and Pattern Recognition (CVPR)*, 2019.

[9] L. Wang, Y. Huang, Y. Hou, S. Zhang, J. Shan, Graph attention convolution for point cloud semantic segmentation, in: *The IEEE Conference on Computer Vision and Pattern Recognition (CVPR)*, 2019.

[10] L. Zhao, X. Peng, Y. Tian, M. Kapadia, D. N. Metaxas, Semantic graph convolutional networks for 3d human pose regression, in: *The IEEE Conference on Computer Vision and Pattern Recognition (CVPR)*, 2019.

[11] Z.-M. Chen, X.-S. Wei, P. Wang, Y. Guo, Multi-label image recognition with graph convolutional networks, in: *The IEEE Conference on Computer Vision and Pattern Recognition (CVPR)*, 2019.

[12] K. Simonyan, A. Zisserman, Very deep convolutional networks for large-scale image recognition, *arXiv preprint arXiv:1409.1556* (2014).

[13] K. He, X. Zhang, S. Ren, J. Sun, Deep residual learning for image recognition, in: *Proceedings of the IEEE conference on computer vision and pattern recognition*, 2016, pp. 770–778.

[14] G. Huang, Y. Sun, Z. Liu, D. Sedra, K. Q. Weinberger, Deep networks with stochastic depth, in: *European conference on computer vision*, Springer, 2016, pp. 646–661.

[15] K. He, X. Zhang, S. Ren, J. Sun, Identity mappings in deep residual networks, in: *European conference on computer vision*, Springer, 2016, pp. 630–645.

[16] G. Huang, Z. Liu, L. Van Der Maaten, K. Q. Weinberger, Densely connected convolutional networks, in: *Proceedings of the IEEE conference on computer vision and pattern recognition*, 2017, pp. 4700–4708.

[17] M. Sandler, A. Howard, M. Zhu, A. Zhmoginov, L.-C. Chen, Mobilenetv2: Inverted residuals and linear bottlenecks, in: *The IEEE Conference on Computer Vision and Pattern Recognition (CVPR)*, 2018.

[18] A. G. Howard, M. Zhu, B. Chen, D. Kalenichenko, W. Wang, T. Weyand, M. Andreetto, H. Adam, Mobilenets: Efficient convolutional neural networks for mobile vision applications, *arXiv preprint arXiv:1704.04861* (2017).

[19] B. Zoph, V. Vasudevan, J. Shlens, Q. V. Le, Learning transferable architectures for scalable image recognition, in: *Proceedings of the IEEE conference on computer vision and pattern recognition*, 2018, pp. 8697–8710.

[20] I. Masi, A. T. Tran, T. Hassner, J. T. Leksut, G. Medioni, Do we really need to collect millions of faces for effective face recognition?, in: *European Conference on Computer Vision*, Springer, 2016, pp. 579–596.

[21] L. Zhang, G.-J. Qi, L. Wang, J. Luo, Aet vs. aed: Unsupervised representation learning by auto-encoding transformations rather than data, in: *Proceedings of the IEEE Conference on Computer Vision and Pattern Recognition*, 2019, pp. 2547–2555.

[22] A. Kolesnikov, X. Zhai, L. Beyer, Revisiting self-supervised visual representation learning, in: *Proceedings of the IEEE conference on Computer Vision and Pattern Recognition*, 2019, pp. 1920–1929.

[23] A. Hamdi, F. Salim, D. Y. Kim, Drotrack: High-speed drone-based object tracking under uncertainty, in: *Proceedings of the IEEE conference on Fuzzy Systems (FUZZ-IEEE)*, 2020.

[24] K. Kolykhalova, G. Gnecco, M. Sanguineti, G. Volpe, A. Camurri, Automated analysis of the origin of movement: An approach based on cooperative games on graphs, *IEEE Transactions on Human-Machine Systems* 50 (6) (2020) 550–560.

- [25] R. Morisi, G. Gnecco, A. Bemporad, A hierarchical consensus method for the approximation of the consensus state, based on clustering and spectral graph theory, *Engineering Applications of Artificial Intelligence* 56 (2016) 157–174.
- [26] D. K. Duvenaud, D. Maclaurin, J. Iparraguirre, R. Bombarell, T. Hirzel, A. Aspuru-Guzik, R. P. Adams, Convolutional networks on graphs for learning molecular fingerprints, in: *Advances in neural information processing systems*, 2015, pp. 2224–2232.
- [27] X. Wang, A. Gupta, Videos as space-time region graphs, in: *Proceedings of the European Conference on Computer Vision (ECCV)*, 2018, pp. 399–417.
- [28] J. Gao, T. Zhang, C. Xu, Watch, think and attend: End-to-end video classification via dynamic knowledge evolution modeling, in: *2018 ACM Multimedia Conference on Multimedia Conference*, ACM, 2018, pp. 690–699.
- [29] J. Gao, T. Zhang, C. Xu, I know the relationships: Zero-shot action recognition via two-stream graph convolutional networks and knowledge graphs, in: *Proceedings of the AAAI Conference on Artificial Intelligence*, Vol. 33, 2019, pp. 8303–8311.
- [30] Y. Shen, H. Li, S. Yi, D. Chen, X. Wang, Person re-identification with deep similarity-guided graph neural network, in: *Proceedings of the European Conference on Computer Vision (ECCV)*, 2018, pp. 486–504.
- [31] H. Fan, H. Ling, Sanet: Structure-aware network for visual tracking, in: *Proceedings of the IEEE Conference on Computer Vision and Pattern Recognition Workshops*, 2017, pp. 42–49.
- [32] M. Li, Z. Ma, Y. G. Wang, X. Zhuang, Fast haar transforms for graph neural networks, *Neural Networks* 128 (2020) 188–198.
- [33] Y. G. Wang, M. Li, Z. Ma, G. Montufar, X. Zhuang, Y. Fan, Haar graph pooling, in: *International conference on machine learning*, PMLR, 2020, pp. 9952–9962.
- [34] P. Veličković, G. Cucurull, A. Casanova, A. Romero, P. Lio, Y. Bengio, Graph attention networks, *arXiv preprint arXiv:1710.10903* (2017).
- [35] D. Atzeni, D. Bacciu, F. Errica, A. Micheli, Modeling edge features with deep bayesian graph networks, in: *2021 International Joint Conference on Neural Networks (IJCNN)*, IEEE, 2021, pp. 1–8.
- [36] S. Pan, R. Hu, G. Long, J. Jiang, L. Yao, C. Zhang, Adversarially regularized graph autoencoder for graph embedding, in: *IJCAI International Joint Conference on Artificial Intelligence*, 2018.
- [37] Z. Cui, Y. Cai, W. Zheng, C. Xu, J. Yang, Spectral filter tracking, *IEEE Transactions on Image Processing* 28 (5) (2018) 2479–2489.
- [38] L. Bertinetto, J. Valmadre, J. F. Henriques, A. Vedaldi, P. H. S. Torr, Fully-convolutional siamese networks for object tracking, *CoRR abs/1606.09549* (2016). [arXiv:1606.09549](http://arxiv.org/abs/1606.09549). URL <http://arxiv.org/abs/1606.09549>
- [39] M.-M. Cheng, Y. Liu, Q. Hou, J. Bian, P. Torr, S.-M. Hu, Z. Tu, Hfs: Hierarchical feature selection for efficient image segmentation, in: *European Conference on Computer Vision*, Springer, 2016, pp. 867–882.
- [40] J. Wang, Y. Jia, X.-S. Hua, C. Zhang, L. Quan, Normalized tree partitioning for image segmentation, in: *2008 IEEE Conference on Computer Vision and Pattern Recognition*, IEEE, 2008, pp. 1–8.
- [41] J. Wang, H. Jiang, Y. Jia, X.-S. Hua, C. Zhang, L. Quan, Regularized tree partitioning and its application to unsupervised image segmentation, *IEEE Transactions on Image Processing* 23 (4) (2014) 1909–1922.
- [42] Y. Chen, M. Rohrbach, Z. Yan, Y. Shuicheng, J. Feng, Y. Kalantidis, Graph-based global reasoning networks, in: *Proceedings of the IEEE Conference on Computer Vision and Pattern Recognition*, 2019, pp. 433–442.
- [43] E. Rublee, V. Rabaud, K. Konolige, G. Bradski, Orb: An efficient alternative to sift or surf, in: *2011 International conference on computer vision*, Ieee, 2011, pp. 2564–2571.
- [44] A. Krizhevsky, G. Hinton, et al., Learning multiple layers of features from tiny images (2009).
- [45] A. Coates, A. Ng, H. Lee, An analysis of single-layer networks in unsupervised feature learning, in: *Proceedings of the fourteenth international conference on artificial intelligence and statistics*, 2011, pp. 215–223.
- [46] T.-Y. Lin, M. Maire, S. Belongie, J. Hays, P. Perona, D. Ramanan, P. Dollár, C. L. Zitnick, Microsoft coco: Common objects in context, in: *European conference on computer vision*, Springer, 2014, pp. 740–755.
- [47] F. Chollet, Xception: Deep learning with depthwise separable convolutions, in: *Proceedings of the IEEE conference on computer vision and pattern recognition*, 2017, pp. 1251–1258.
- [48] C. Szegedy, V. Vanhoucke, S. Ioffe, J. Shlens, Z. Wojna, Rethinking the inception architecture for computer vision, in: *Proceedings of the IEEE conference on computer vision and pattern recognition*, 2016, pp. 2818–2826.
- [49] A. Grover, J. Leskovec, node2vec: Scalable feature learning for networks, in: *Proceedings of the 22nd ACM SIGKDD international conference on Knowledge discovery and data mining*, ACM, 2016, pp. 855–864.
- [50] T. N. Kipf, M. Welling, Semi-supervised classification with graph convolutional networks, in: *International Conference on Learning Representations (ICLR)*, 2017.
- [51] D. Berthelot, N. Carlini, I. Goodfellow, N. Papernot, A. Oliver, C. A. Raffel, Mixmatch: A holistic approach to semi-supervised learning, in: *Advances in Neural Information Processing Systems*, Vol. 32, Curran Associates, Inc., 2019.
- [52] Z. Huang, S. Liang, M. Liang, H. Yang, Dianet: Dense-and-implicit attention network, in: *Proceedings of the AAAI Conference on Artificial Intelligence*, Vol. 34, 2020, pp. 4206–4214.
- [53] W. Deng, Q. Feng, L. Gao, F. Liang, G. Lin, Non-convex learning via replica exchange stochastic gradient mcmc, in: *International Conference on Machine Learning*, PMLR, 2020, pp. 2474–2483.
- [54] G. Chrysos, S. Moschoglou, G. Bouritsas, J. Deng, Y. Panagakis, S. P. Zafeiriou, Deep polynomial neural networks, *IEEE Transactions on Pattern Analysis and Machine Intelligence* (2021).
- [55] G. Wang, K. Wang, L. Lin, Adaptively connected neural networks, in: *Proceedings of the IEEE/CVF Conference on Computer Vision and Pattern Recognition*, 2019, pp. 1781–1790.
- [56] J.-B. Cordonnier, A. Loukas, M. Jaggi, On the relationship between self-attention and convolutional layers, in: *International Conference on Learning Representations*, 2020.
- [57] G.-J. Qi, Loss-sensitive generative adversarial networks on lipschitz densities, *International Journal of Computer Vision* 128 (5) (2020) 1118–1140.
- [58] R. D. Hjelm, A. Fedorov, S. Lavoie-Marchildon, K. Grewal, P. Bachman, A. Trischler, Y. Bengio, Learning deep representations by mutual information estimation and maximization, in: *International Conference on Learning Representations*, 2019.
- [59] A. Makhzani, J. Shlens, N. Jaitly, I. Goodfellow, B. Frey, Adversarial autoencoders, *arXiv preprint arXiv:1511.05644* (2015).
- [60] D. P. Kingma, M. Welling, Auto-encoding variational bayes, in: *International Conference on Learning Representations (ICLR)*, 2014.
- [61] E. Dupont, A. Doucet, Y. W. Teh, Augmented neural odes, in: H. Wallach, H. Larochelle, A. Beygelzimer, F. d’Alché-Buc, E. Fox, R. Garnett (Eds.), *Advances in Neural Information Processing Systems 32*, Curran Associates, Inc., 2019, pp. 3140–3150.
- [62] V. Dumoulin, I. Belghazi, B. Poole, O. Mastropietro, A. Lamb, M. Arjovsky, A. Courville, Adversarially learned inference, *arXiv preprint arXiv:1606.00704* (2016).
- [63] Y. Yu, Z. Gong, P. Zhong, J. Shan, Unsupervised representation learning with deep convolutional neural network for remote sensing images, in: *International Conference on Image and Graphics*, Springer, 2017, pp. 97–108.
- [64] E. Oyallon, S. Mallat, Deep roto-translation scattering for object classification, in: *Proceedings of the IEEE Conference on Computer Vision and Pattern Recognition*, 2015, pp. 2865–2873.
- [65] A. Dosovitskiy, J. T. Springenberg, M. Riedmiller, T. Brox, Discriminative unsupervised feature learning with convolutional neural networks, in: *Advances in neural information processing systems*, 2014, pp. 766–774.
- [66] S. Gonzalez, R. Mikkulainen, Improved training speed, accuracy, and data utilization through loss function optimization, in: *2020 IEEE Congress on Evolutionary Computation (CEC)*, IEEE, 2020, pp. 1–8.
- [67] S. Sabour, N. Frosst, G. E. Hinton, Dynamic routing between capsules, in: *Advances in neural information processing systems*, 2017, pp. 3856–3866.
- [68] D. Hendrycks, K. Gimpel, A baseline for detecting misclassified and out-of-distribution examples in neural networks, in: *International Conference on Learning Representations (ICLR)*, 2017.
- [69] Z. Liao, G. Carneiro, On the importance of normalisation layers in deep learning with piecewise linear activation units, in: *2016 IEEE Winter Conference on Applications of Computer Vision (WACV)*, IEEE, 2016, pp. 1–8.
- [70] C.-Y. Lee, S. Xie, P. Gallagher, Z. Zhang, Z. Tu, Deeply-supervised nets, in: *Artificial intelligence and statistics*, PMLR, 2015, pp. 562–570.
- [71] M. Courbariaux, Y. Bengio, J.-P. David, Binaryconnect: Training deep neural networks with binary weights during propagations, in: *NIPS*, 2015.

- [72] D. Misra, Mish: A self regularized non-monotonic neural activation function, in: British Machine Vision Conference (BMVC), 2020.
- [73] C. Trabelsi, O. Bilaniuk, Y. Zhang, D. Serdyuk, S. Subramanian, J. F. Santos, S. Mehri, N. Rostamzadeh, Y. Bengio, C. J. Pal, Deep complex networks, in: International Conference on Learning Representations, 2018.
- [74] H. Lee, H.-E. Kim, H. Nam, Srm: A style-based recalibration module for convolutional neural networks, in: Proceedings of the IEEE/CVF International Conference on Computer Vision, 2019, pp. 1854–1862.
- [75] E. Real, S. Moore, A. Selle, S. Saxena, Y. L. Suematsu, J. Tan, Q. V. Le, A. Kurakin, Large-scale evolution of image classifiers, in: International Conference on Machine Learning, PMLR, 2017, pp. 2902–2911.
- [76] Y. Zheng, R. Zhang, Y. Mao, Regularizing neural networks via adversarial model perturbation, in: The IEEE Conference on Computer Vision and Pattern Recognition (CVPR), 2021.
- [77] S. Zagoruyko, N. Komodakis, Wide residual networks, arXiv preprint arXiv:1605.07146 (2016).
- [78] I. Higgins, L. Matthey, A. Pal, C. Burgess, X. Glorot, M. Botvinick, S. Mohamed, A. Lerchner, beta-vae: Learning basic visual concepts with a constrained variational framework, in: International Conference on Learning Representations (ICLR), 2017.
- [79] A. A. Alemi, I. Fischer, J. V. Dillon, K. Murphy, Deep variational information bottleneck, arXiv preprint arXiv:1612.00410 (2016).
- [80] J. Carranza-Rojas, S. Calderon-Ramirez, A. Mora-Fallas, M. Granados-Menani, J. Torrents-Barrena, Unsharp masking layer: injecting prior knowledge in convolutional networks for image classification, in: International Conference on Artificial Neural Networks, Springer, 2019, pp. 3–16.
- [81] L. Hertel, E. Barth, T. Käster, T. Martinetz, Deep convolutional neural networks as generic feature extractors, in: 2015 International Joint Conference on Neural Networks (IJCNN), 2015, pp. 1–4. doi: 10.1109/IJCNN.2015.7280683.
- [82] D.-A. Clevert, T. Unterthiner, S. Hochreiter, Fast and accurate deep network learning by exponential linear units (elus), arXiv preprint arXiv:1511.07289 (2015).
- [83] P. Bojanowski, A. Joulin, Unsupervised learning by predicting noise, arXiv preprint arXiv:1704.05310 (2017).
- [84] Z. Shao, J. Yang, Increasing the trustworthiness of deep neural networks via accuracy monitoring, in: Proceedings of the Workshop on Artificial Intelligence Safety 2020 (co-located with IJCAI-PRICAI 2020), 2020.
- [85] E. Oyallon, E. Belilovsky, S. Zagoruyko, Scaling the scattering transform: Deep hybrid networks, in: Proceedings of the IEEE international conference on computer vision, 2017, pp. 5618–5627.
- [86] B. Miclut, Committees of deep feedforward networks trained with few data, *Pattern Recognition* (2014) 736–742 doi:10.1007/978-3-319-11752-2_62.
- [87] D. Wang, X. Tan, Unsupervised feature learning with c-svddnet, *Pattern Recogn.* 60 (C) (2016) 473–485. doi:10.1016/j.patcog.2016.06.001.
- [88] C. Luo, J. Zhan, L. Wang, W. Gao, Extended batch normalization, arXiv preprint arXiv:2003.05569 (2020).
- [89] L. Ruthotto, E. Haber, Deep neural networks motivated by partial differential equations, *Journal of Mathematical Imaging and Vision* (2019) 1–13.
- [90] M. Ye, J. Shen, Probabilistic structural latent representation for unsupervised embedding, in: Proceedings of the IEEE/CVF Conference on Computer Vision and Pattern Recognition (CVPR), 2020.
- [91] S. Löwe, P. O’Connor, B. S. Veeling, Putting an end to end-to-end: Gradient-isolated learning of representations., in: *NeurIPS*, 2019, pp. 3033–3045.
- [92] T. Robert, N. Thome, M. Cord, Hybridnet: Classification and reconstruction cooperation for semi-supervised learning, in: Proceedings of the European Conference on Computer Vision (ECCV), 2018, pp. 153–169.
- [93] M. Ye, J. Shen, Probabilistic structural latent representation for unsupervised embedding, in: Proceedings of the IEEE/CVF conference on computer vision and pattern recognition, 2020, pp. 5457–5466.
- [94] B. Chang, L. Meng, E. Haber, L. Ruthotto, D. Begert, E. Holtham, Reversible architectures for arbitrarily deep residual neural networks, in: Proceedings of the AAAI Conference on Artificial Intelligence, Vol. 32, 2018.
- [95] X. Ji, J. F. Henriques, A. Vedaldi, Invariant information clustering for unsupervised image classification and segmentation, in: Proceedings of the IEEE/CVF International Conference on Computer Vision, 2019, pp. 9865–9874.
- [96] I. Sosnovik, M. Szmaja, A. Smeulders, Scale-equivariant steerable networks, in: International Conference on Learning Representations, 2020.
- [97] Z. Lu, K. Deb, E. Goodman, W. Banzhaf, V. N. Boddeti, Nsganetv2: Evolutionary multi-objective surrogate-assisted neural architecture search, in: European Conference on Computer Vision, Springer, 2020, pp. 35–51.
- [98] K. Sohn, D. Berthelot, N. Carlini, Z. Zhang, H. Zhang, C. A. Raffel, E. D. Cubuk, A. Kurakin, C.-L. Li, Fixmatch: Simplifying semi-supervised learning with consistency and confidence, in: H. Larochelle, M. Ranzato, R. Hadsell, M. F. Balcan, H. Lin (Eds.), *Advances in Neural Information Processing Systems*, Vol. 33, Curran Associates, Inc., 2020, pp. 596–608.
- [99] M. Chen, A. Radford, R. Child, J. Wu, H. Jun, D. Luan, I. Sutskever, Generative pretraining from pixels, in: International Conference on Machine Learning, PMLR, 2020, pp. 1691–1703.
- [100] B. Perozzi, R. Al-Rfou, S. Skiena, Deepwalk: Online learning of social representations, in: Proceedings of the 20th ACM SIGKDD international conference on Knowledge discovery and data mining, ACM, 2014, pp. 701–710.